AGU PUBLICATIONS

JGR

Journal of Geophysical Research: Space Physics

RESEARCH ARTICLE

10.1002/2017JA023954

The quasi-6 day wave and its interactions with solar tides

Jeffrey M. Forbes[1] and **Xiaoli Zhang**[1]

[1] Department of Aerospace Engineering Sciences, University of Colorado Boulder, Boulder, Colorado, USA

Key Points:
- Climatological characteristics of the quasi-6 day wave and their propagation features are revealed
- Evidences show secondary waves resulting from quasi-6 day waves nonlinear interactions with solar tides are significant
- The secondary waves have different latitude-height structures from those primary waves; both can affect ionosphere in similar ways

Supporting Information:
- Supporting Information S1

Correspondence to:
J. M. Forbes,
forbes@colorado.edu

Citation:
Forbes, J. M., and X. Zhang (2017), The quasi-6 day wave and its interactions with solar tides, *J. Geophys. Res. Space Physics*, *122*, 4764–4776, doi:10.1002/2017JA023954.

Received 25 JAN 2017
Accepted 9 MAR 2017
Accepted article online 16 MAR 2017
Published online 27 APR 2017

Abstract Thermosphere Ionosphere Mesosphere Energetics and Dynamics/Sounding of the Atmosphere using Broadband Emission Radiometry (TIMED/SABER) temperature measurements between 20 and 110 km altitude and ±50° latitude during 2002–2015 are employed to reveal the climatological characteristics of the quasi-6 day wave (Q6DW) and evidence for secondary waves (SW) resulting from its nonlinear interactions with solar tides. The mean period is 6.14d with a standard deviation (σ) of 0.26d. Multiyear-mean maximum amplitudes (3–5 K, $\sigma \sim 4$ K) occur within the mesosphere-lower thermosphere (MLT) region between 75 and 100 km during day of year (DOY) 60–120 and 180–300 in the Northern Hemisphere and DOY 0–110 and 200–300 in the Southern Hemisphere. Amplitudes approach 10 K in some individual years. At midlatitudes downward phase progression exists from 100 to 35 km with a mean vertical wavelength of about 70 km. Signatures of SW due to Q6DW-tide interactions appear at distinct space-based zonal wave numbers (k_s) in temperature spectra constructed in the reference frame of the TIMED orbit. However, SW produced by several different tides can collapse onto the same (k_s) value, rendering their relative contributions indistinguishable. Nevertheless, by determining the space-based wave amplitudes attached to these values of (k_s), and demonstrating that they are a large fraction of the interacting wave amplitudes, we conclude that the aggregate contributions of the SW to the overall wave spectrum must be significant. Because the SW have periods, zonal wave numbers, and latitude-height structures different from those of the primary waves, they contribute additionally to the complexity of the wave spectrum. This complexity is communicated to the ionosphere through collisions or through the dynamo electric fields generated by the total wave spectrum.

1. Introduction

The primary mechanism through which energy and momentum are transferred from the lower atmosphere to the upper atmosphere and ionosphere is through the generation and propagation of waves. The wave spectrum entering the thermosphere from below mainly consists of gravity waves, solar and lunar tides, planetary waves (PW), and ultrafast Kelvin waves (UFKW). The climatological spectrum of upward propagating tides at 110 km is now reasonably well known [*Truskowski et al.*, 2014] and consists of eastward and westward propagating diurnal, semidiurnal, and terdiurnal components spanning a spectrum of zonal wave numbers. The UFKW are eastward propagating with periods between about 2 and 5 days in the mesosphere-lower thermosphere (MLT) region (80–110 km), with zonal wave numbers of $s = -1$ and $s = -2$ [*Forbes et al.*, 2009]. PW with periods near 2, 6, 10, and 16 days (hereafter Q2DW, Q6DW, Q10DW, and Q16DW) are also common features of the MLT [e.g., *Moudden and Forbes*, 2014; *Tunbridge et al.*, 2011; *Espy and Witt*, 1996; *Forbes and Zhang*, 2015; *Miyoshi*, 1999; *Liu et al.*, 2004; *Sassi et al.*, 2012, 2013, and references therein] and are generally recognized as the atmospheric manifestations of resonant or normal modes of classical wave theory [*Longuet-Higgins*, 1968; *Forbes*, 1995]. The Q6DW, Q10DW, and Q16DW are westward propagating with $s = 1$, while the Q2DW consists mainly of $s = 3$ and sometimes $s = 2$ and 4. The Q2DW and Q6DW are the most robust and well studied of these. The present study focuses on the Q6DW and, in particular, its nonlinear interaction with atmospheric tides.

One of the issues often raised in connection with the Q6DW is exactly what period should be ascribed to this wave, given that classical wave theory on a rotating sphere (which neglects the effects of mean winds) predicts atmospheric resonance to occur close to 5 days. In fact some authors refer to this oscillation as the 5 day wave even though their data analyses indicate that the period is actually 6 days or more [e.g., *Wu et al.*, 1994; *Riggin et al.*, 2006]. One reason for this is that the horizontal structure of the wave derived from MLT data is very well approximated by that of the first symmetric Rossby normal mode with 5 day period and zonal wave

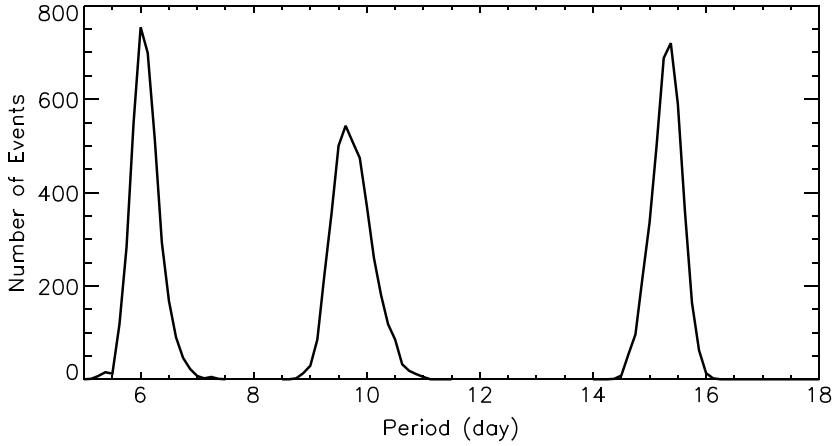

Figure 1. Wave periods obtained for westward propagating waves with zonal wave number $s = 1$. These results correspond to fits performed between ±50° latitude and from 20–100 km altitude during 2002–2015, and only correspond to wave amplitudes greater than 0.5 K. The mean values (standard deviations) for each peak are 6.14d(0.26d), 9.81d(0.35d), and 15.4(0.26d).

number $s = 1$. However, as noted by *Forbes* [1995], a simple Doppler shift correction to classical wave theory places the period near 5.6 days. It is to be expected that the period of the oscillation will in fact be dependent on the background wind and thermal structure [*Salby*, 1981]. There is also evidence that instability-driven amplification of this wave exists, with maximum growth rate at 6 days or longer [*Meyer and Forbes*, 1997; *Lieberman et al.*, 2003]. In the present paper we present experimental evidence favoring a multiyear-mean period of 6.14 days and thus the label "Q6DW," but a range of periods around 6 days also exists, particularly within any given year.

Several comprehensive studies have been performed that delineate the vertical and latitudinal structure of the Q6DW in the stratosphere [*Hirooka and Hirota*, 1984] and in the MLT [*Wu et al.*, 1994; *Talaat et al.*, 2001, 2002; *Lieberman et al.*, 2003; *Riggin et al.*, 2006; *Jiang et al.*, 2008; *Pancheva et al.*, 2009; *Gu et al.*, 2014]. As noted above, MLT latitude structures of temperature, zonal, and meridional winds conform well with those of the 5 day oscillation from classical wave theory (see Figure 1). Maximum amplitudes occur around the equinoxes, and as noted by *Pancheva et al.* [2009], the vertical structure is characterized by maxima near 80–90 km and 100–115 km. Vertical wavelengths are generally quoted in the range of 60–70 km and thus inconsistent with the infinite vertical wavelength predicted by classical wave theory. Phase progression with height is, however, generally consistent with that of a forced wave or the presence of dissipation [*Lindzen and Blake*, 1972; *Salby*, 1979], which is neglected in classical theory.

A recent and important revelation concerning the Q6DW is its ionospheric effects. For instance, *Gu et al.* [2014] demonstrate a Q6DW in total electron content (TEC) coincident with a strong Q6DW event in the MLT. *Gan et al.* [2015] conclude that 6 day variations in TEC were communicated to the ionosphere through $[O]/[N_2]$ variations (and related ionospheric chemistry) due to dissipation of the Q6DW in the lower thermosphere; the $[O]/[N_2]$ variations were measured by Thermosphere Ionosphere Mesosphere Energetics and Dynamics/Global Ultraviolet Imager (TIMED/GUVI) and the TEC from Global Navigation Satellite Systems measurements. *Gan et al.* [2016] present numerical modeling evidence that the Q6DW produces ionospheric variability through dynamo electric fields generated both directly and through modulation of vertically propagating tides. *Liu et al.* [2010] demonstrated a Q6DW modulation of the wave-4 longitudinal structure of the peak height (h_mF_2) of the equatorial ionosphere as observed in COSMIC (Constellation Observing System for Meteorology, Ionosphere, and Climate) data. They ascribed this observation to plasma drifts/dynamo electric fields due to the eastward propagating diurnal tide with $s = -3$ (DE3), which was modulated by the Q6DW observed in the MLT. *Pancheva et al.* [2008] and *Elhawary and Forbes* [2016] also found evidence for Q6DW effects in the equatorial and low-latitude ionosphere, namely, in ground magnetic data that reflect the presence of *E* region currents associated with the dynamo-driven electric fields. *Pancheva et al.* [2008]

furthermore showed that at tropical latitudes (near ±20° geographic) Q6DW modulation of the tides was evident, whereas the equatorial (±10° geographic) stations mainly reflected the presence of the Q6DW itself.

Based on the above observations, it appears that the Q6DW periodicity can be impressed upon the ionosphere in at least three ways: through composition effects associated with dissipation of the wave; through the generation of dynamo electric fields by a Q6DW that directly penetrates into the *E* region; and through the Q6DW modulation of solar tides that then propagate into the *E* region and generate dynamo electric fields [*Forbes*, 1996]. Although the aforementioned observations and theory [*Meyer and Forbes*, 1997; *Pedatella et al.*, 2012] provide evidence that the Q6DW indeed penetrates above 100 km, there is scant observational evidence for Q6DW modulation of atmospheric tides [e.g., *Clark and Bergin*, 1997; *Canziani*, 1994a, 1994b; *Pancheva*, 2001] as compared, for instance, with that of the 2 day wave [*Beard et al.*, 1999; *Cevolani and Kingsley*, 1992; *Huuskonen et al.*, 1991; *Pancheva*, 2006; *Pancheva and Mitchell*, 2004; *Forbes and Moudden*, 2012]. Nevertheless, recent modeling [*Pedatella et al.*, 2012] suggests that strong Q6DW-tide interactions can potentially occur, resulting in significant-amplitude secondary waves (SW) that propagate into the dynamo region. There is thus a need to provide experimental verification of this modeling result.

The main purpose of the present paper is to pursue observational evidence for the existence of Q6DW-tide interactions in the MLT using Sounding of the Atmosphere using Broadband Emission Radiometry (SABER) temperature measurements from the TIMED mission covering 2002–2015. A second objective is to provide the first multiyear climatological perspective of the Q6DW. The following two sections describe the SABER data and the methodology used to extract the Q6DW, and the main climatological features of the Q6DW as provided by SABER temperature measurements. The subsequent section reviews modeling evidence for Q6DW modulation of atmospheric tides [*Pedatella et al.*, 2012] and our approach for extracting related observational evidence from TIMED/SABER temperature measurements. Results are presented in section 4, and section 5 is reserved for summary and conclusions.

Throughout this paper, the notation DW*s*(SW*s*) or DE*s*(SE*s*) is used to denote a Westward or Eastward propagating Diurnal(Semidiurnal) tide, respectively, with zonal wave number = *s*. Zonally symmetric oscillations are denoted by D0(S0).

2. Data and Method of Analysis

2.1. SABER Temperature Measurements

In this study we analyze SABER Version 1.07 temperature measurements covering 2002–2015, extending from 20 km up to 100 km. Below 100–110 km is where the SABER temperature retrievals become independent of external assumptions [*Mertens et al.*, 2001; *Remsberg et al.*, 2008]. Our derived Q6DW amplitudes become less well defined in terms of latitude structure at 110 km as opposed to 100 km, so we use 100 km as the upper limit for this part of our analysis in subsection 2.2. In addition, we restrict analysis of SABER data to latitudes equatorward of ±50° latitude where sampling is unaffected by yaw maneuvers. Data coverage in UT and longitude within this latitude range is more or less continuous, and relatively few data gaps exist, except near noon where SABER does not take measurements.

2.2. Extraction of the Q6DW

We follow the same procedure here to extract the Q6DW from SABER measurements as described by *Forbes and Zhang* [2015] for the quasi-10 day wave (Q10DW). First, 60 day mean migrating and nonmigrating tides are removed according to the method described by *Forbes et al.* [2008] and *Truskowski et al.* [2014]. Residuals obtained by subtracting the tidal components are fit for the Q6DW within 20 day sliding windows with periods ranging between 4.0 and 8.0 days in increments of 0.125 day. At any given height and latitude the Q6DW amplitude and phase is obtained from the fit with the largest amplitude. *Forbes and Zhang* [2015] discuss the uncertainties associated with the amplitudes and phases by the present method, and the same estimates apply here. That is, 1 sigma uncertainties range from about 0.1 to 0.2 K between 20 and 40 km altitude, to 0.2 to 0.4 K between 60 and 80 km, to about 0.3–0.4 K at 80 km and 0.5 to 0.7 K at 100 km. Uncertainties in phase are generally less than 0.5 day. See *Forbes and Zhang* [2015] for more details.

2.3. PW-Tide Interactions

A method has been developed that provides evidence for the existence of PW-tide interactions, and that can be used to quantify the magnitudes of SW produced by these interactions. This methodology was

originally derived to explain density variability in the lower thermosphere of Mars [*Moudden and Forbes*, 2010, 2011a, 2011b] but was later applied to the quasi-2 day wave at Earth [*Forbes and Moudden*, 2012; *Pedatella and Forbes*, 2012; *Moudden and Forbes*, 2014]. The methodology consists of ordering data in pseudolongitude, the traditional longitude incremented by 2π times the number of Earth revolutions since a given time. This arrangement eliminates the fictitious discontinuity at 0/360° longitude.

Within this methodology the mathematical description of tides and PW remains unchanged from normal conventions. The time longitude dependence of a tide is thus $\cos(n\Omega t + s\lambda_p - \phi)$ where $\Omega = 2\pi d^{-1}$, t = UT, $n = 1$ and 2 for diurnal and semidiurnal tides, respectively, s is the zonal wave number, and λ_p is now the pseudolongitude instead of just longitude. The same notation applies to a PW: $\cos(\delta\Omega t + m\lambda_p - \phi)$ describes a single PW having a frequency $\delta\Omega$ and a zonal wave number m; e.g., in the case of a 2 day wave, $\delta = 0.5$. The interaction of a tide and PW in the above form yields SW with frequencies equal to $n\Omega \pm \delta\Omega$ and zonal wave numbers equal to $s \pm m$, respectively [*Teitelbaum and Vial*, 1991]; these are often referred to as sum(+) and difference(−) SW, hereafter SW^+ and SW^-.

When sampled at a nearly constant local time (i.e., quasi-Sun-synchronous satellite like TIMED), a tide appears as a wave in the form $\cos[n\Omega t_L + (s-n)\lambda_p - \phi]$, a PW in the form $\cos[\delta\Omega t_L + (m-\delta)\lambda_p - \phi]$, and a SW in the form $\cos[(n \pm \delta)\Omega t_L + (s \pm m - n \mp \delta)\lambda_p - \phi]$. (As shown by *Forbes and Moudden* [2012], the local time precession of TIMED is too slow to appreciably affect the location of the spectral peaks.) These various space-based zonal wave numbers $[k_s = (s-n), (m-\delta), (s-n) \pm (m-\delta)]$ for different existing tides, PWs, and their SW each contribute to the zonal variability in any atmospheric field. Additional attributes of the method are that data from either ascending or descending parts of the orbit can be used and that interactions between diurnal, semidiurnal, and terdiurnal tides with any longer-period coexisting PW appear somewhere in the spectra.

Spectral analysis of a given time series of space-based measurements as described above can reveal the significant peaks of $k_s = (s-n), (m-\delta), (s-n) \pm (m-\delta)$. Note that tides appear as integers, and one cannot differentiate between a PW and the PW modulation of a migrating tide ($s - n = 0$). As demonstrated in section 4, a further shortcoming is that for a given PW period a SW spectral peak k_s can result from interactions between several nonmigrating tidal components and that PW; i.e., mathematically unique solutions usually do not exist, although other information can often be used to narrow the possibilities.

By way of example analogous to the present application, the reader is referred to the work of *Gasperini et al.* [2015], which illustrates pseudolongitude spectra of SABER temperatures containing DE3, a 3.5 day UFKW, and the 2 SW resulting from their interaction: SW^+ has a period of 0.77 day, $s = -4$ and $k_s = 5.3$, while SW^- has a period of 1.43 days, $s = -2$, and $k_s = 2.7$. Although these SW are not retrievable from normal time series analyses, they are identifiable in the pseudolongitude spectrum due to the specificity of their space-based wave numbers. These authors also demonstrate existence of these waves near 260 km in densities measured by the GOCE satellite, and that the SW contribute significantly to the total spatial-temporal variability of temperatures at 100 km and densities at 260 km.

3. Climatological Characteristics of the Q6DW

Figure 1 illustrates the distribution of Q6DW wave periods obtained from the fitting procedure described in section 2.2, taking only those values when the amplitude exceeds 0.5 K. The mean value of the Q6DW period is 6.14 days with a standard deviation (σ) of 0.26 day. This value does not change appreciably if the altitude range is restricted to 60–100 km or 80–100 km. The climatological wave periods for the Q10DW and Q16DW obtained from this data set are also included in this figure, which are 9.81 days ($\sigma = 0.35$) for the Q10DW [*Forbes and Zhang*, 2015] and 15.35 days ($\sigma = 0.26$) for the Q16DW. Mean wave periods within any given year can differ somewhat from these values.

Multiyear mean Q6DW amplitudes are illustrated in Figure 2. Superimposed on these plots is the latitude dependence of temperature for the 5 day normal mode as predicted by classical wave theory, as shown in Figure 3 which also includes the corresponding zonal and meridional wind expansion functions. Figure 2 (left column) illustrates latitude versus day of year (DOY) amplitudes of the Q6DW at 44 km, 80 km, 90 km, and 100 km altitudes. Only amplitudes greater than 0.5 K are plotted as this is the minimum estimated detectable amplitude. We note general correspondence with the 5 day Hough function in that amplitudes are minimum

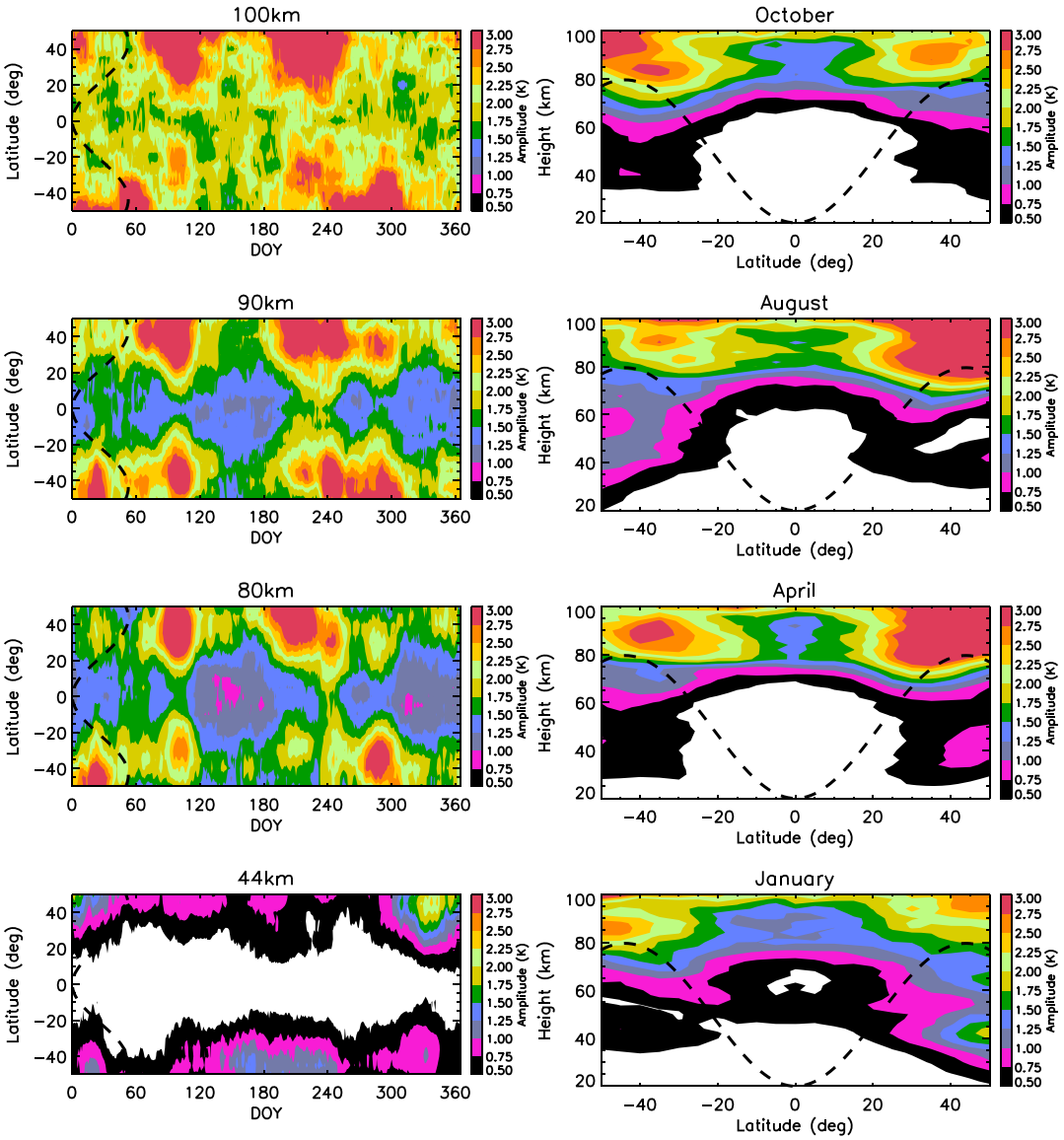

Figure 2. (left column) Latitude versus day-of-year structures of multiyear average (2002–2015) Q6DW temperature amplitudes at 44 km, 80 km, 90 km, and 100 km. (right column) Height versus latitude structures of Q6DW temperature amplitudes for the 20 day fitting windows centered on 15 January, 15 April, 15 August, and 15 October. All amplitudes represent averages over 2002–2015. Dashed black lines correspond to Hough mode shape for 5 day normal mode presented in Figure 3. White areas correspond to amplitudes less than 0.5 K.

near the equator and tend toward larger values between ±30 and 50° latitude. In the Northern Hemisphere (NH) MLT maxima occur mainly between DOY 60–120 and 180–240 with a smaller burst of activity near DOY 270, which is quite different from that at 44 km, where the largest amplitudes occur between DOY 300–360. The difference may lie in the fact that instability conditions mainly control the seasonal behavior of the Q6DW in the MLT. Similarly, in the Southern Hemisphere (SH), amplitude maxima appear between DOY 240–300, but this is a minimum time of Q6DW activity at 44 km. The same contrast exits near DOY 90.

Figure 2 (right column) displays height versus latitude structures of Q6DW mean amplitudes for fitting windows centered on 15 January, 15 April, 15 August, and 15 October. These distributions do not reveal any correlation in Q6DW amplitudes between the stratosphere and MLT and in fact tend to show separate stratosphere and MLT regimes of Q6DW activity; that is, the strongest MLT amplitudes do not occur with the strongest stratospheric amplitudes. See, for instance, Q6DW amplitudes near 44 km in SH August, NH April, and both NH and SH in January.

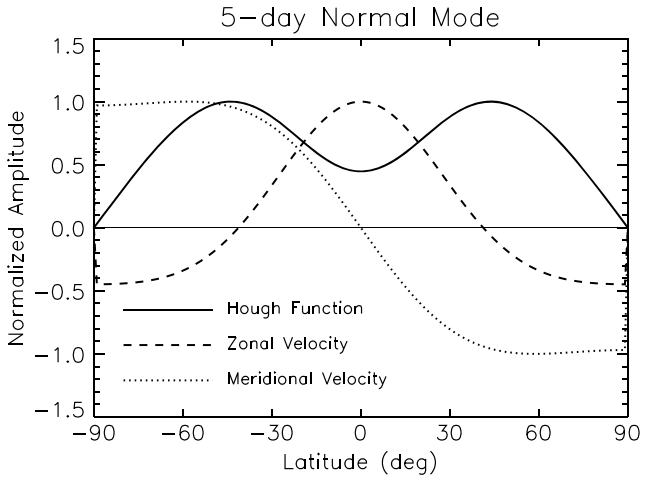

Figure 3. Hough function (solid) and zonal (dashed) and meridional (dotted) velocity expansion functions for the 5 day normal mode from classical wave theory on a sphere.

Height versus DOY plots of the multiyear mean Q6DW temperature amplitude are depicted in Figure 4 at −40°, 0°, and +40° latitude. In contrast to ±40° latitude, intraannual variations are not very prominent at the equator. The lack of correlation between stratosphere and MLT Q6DW amplitudes is particularly evident, especially in the SH where there is some degree of anticorrelation. The Q6DW also exhibits significant interannual variability, as illustrated in Figure S1 in the supporting information. Amplitudes range from weak amplitudes (<3 K) on a global scale during 2008 to rather strong amplitudes (8 K) in both hemispheres during 2004.

Figure 5 illustrates vertical structures of multiyear mean Q6DW amplitudes and phases at +40° and −40° latitude for the fitting window centered on 1 April, when similar MLT structures are seen in both hemispheres. Figure 5 (left) shows amplitude profiles corresponding to fits assuming a specified wave period of 6.0 days, so that phase comparisons between the various fits can be appropriately made. The displayed amplitudes only differ slightly from those displayed in Figures 2 and 4, and which correspond to the largest amplitude obtained within a range of assumed wave periods. We note the different vertical structures of the Q6DW between hemispheres, and the standard deviations (σ) of order 4 K which are indicative of large interannual variability. Below 80–90 km the SH amplitude profile does not depart appreciably from the exponential growth expected for an atmospheric normal mode in the absence of mean winds and dissipation (dotted line in Figure 5, left), but a precipitous decrease in amplitude occurs above 90 km. On the other hand, the NH profile exhibits double maxima (82 km and 96 km) and amplitudes significantly in excess (50–100%) of those expected from simple wave theory. These larger amplitudes could be a signature of instability-driven amplification [*Meyer and Forbes*, 1997]. These conclusions should of course be viewed in the context of the large standard deviations attached to the displayed amplitudes.

Figure 5 (middle) displays multiyear mean Q6DW phase differences between +40° and −40° latitude corresponding to the amplitudes plotted in Figure 5 (left). The relatively small departures from zero phase difference point to the quasi-symmetric nature of the Q6DW, at least for near-equinox conditions where the effects of asymmetric mean winds are minimized. Under these conditions, therefore, and apart from some MLT amplitude amplification in the NH, the behavior of the Q6DW approximates that of the 5 day wave from classical wave theory on a sphere.

Figure 5 (right) depicts phase differences relative to those at 40 km altitude in each hemisphere. The downward phase progression with height (vertical wavelength ≈70 km), which is about the same in both hemispheres, is consistent with upward phase propagation and thus a lower atmosphere source for the wave. This feature represents a departure from classical wave theory predictions of an infinite vertical wavelength (zero phase progression) for an atmospheric normal mode in the absence of mean winds and dissipation. The presence of some phase progression with height is consistent with the presence of dissipation [*Lindzen and Blake*, 1972].

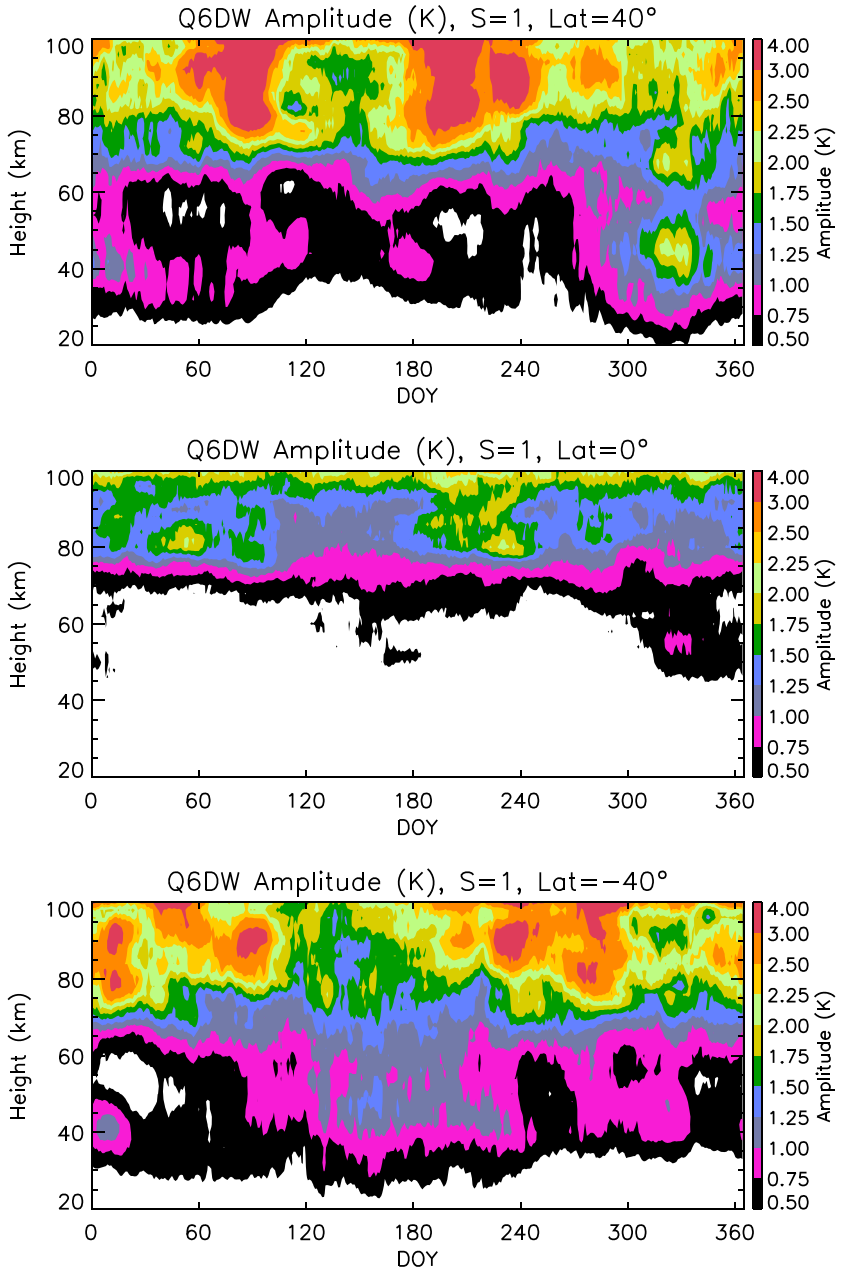

Figure 4. Height versus DOY structures of multiyear average (2002–2015) Q6DW temperature amplitudes at (top) +40°, (middle) 0°, and (bottom) −40° latitude. White areas correspond to amplitudes less than 0.5 K.

4. Evidence for Q6DW-Tide Nonlinear Interactions

The Lomb-Scargle spectral method was applied to the database of temperature residuals (section 2.2) ordered in pseudolongitude (section 2.3) to provide a survey of spectral peaks that could be associated with Q6DW-tide interactions. The occurrence of such interactions was indeed found to be very common, although during many months little evidence can be found for significant SW peaks due to PW-tide interactions. Monthly spectra for the whole database at 80, 90, 100, and 110 km are provided in Figures S2a–S2d, respectively. Figure 6 shows some typical examples, chosen to represent the range of spectral peaks that are distributed throughout the database. The period of the Q6DW is taken to be the mean period depicted in Figure 1, i.e., 6.14 days. Recall that evidence of such interactions is provided by the existence of peaks in the pseudolongitude spectra at $|(s-n)\pm(m-\delta)|$ or $|(s-n)\pm 0.84|$ where $m = 1$ and $\delta = \frac{1}{6.14} = 0.16$ for the Q6DW.

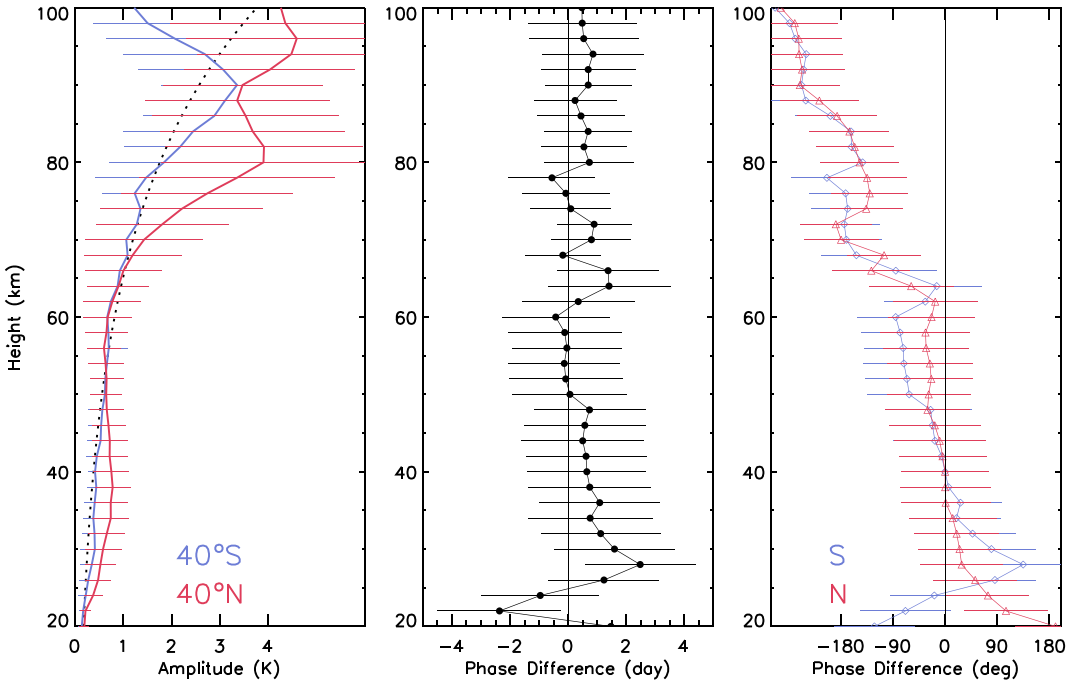

Figure 5. (left) Q6DW temperature amplitudes for the fitting windows centered on 1 April versus height, averaged over 2002–2015 at +40° (red) and −40° (blue) latitude. Also shown is the theoretical height dependence for a normal mode (dotted black line), namely, $e^{\kappa z}$, where z = altitude and $\kappa = 0.29$. (middle) Mean phase differences between +40° and −40° latitude corresponding to the Q6DW wave amplitudes in Figure 5 (left). (right) Mean phase differences at all heights from those at 40 km altitude in each respective hemisphere. Horizontal lines in all panels represent standard deviations of multiyear means, a measure of interannual variability.

For the diurnal ($n = 1$) and semidiurnal ($n = 2$) tides that are commonly seen in MLT data [e.g., *Truskowski et al.*, 2014], the corresponding pseudolongitude spectral peaks arising due to nonlinear interaction with the Q6DW are provided in Table 1. It is immediately obvious that any given peak has its potential origins in multiple tidal interactions with the Q6DW. Taking $k_s = 1.16$ as an example, which is one of the more prevalent spectral peaks to emerge from our survey of SABER temperature data, it reflects the presence of Q6DW interactions with any of the following tides: DE1, S0, SW4 (or any tide that possesses a longitudinal wave number $|(s - n) = 2|$ from a quasi-Sun-synchronous orbit). Also included in Table 1 are the periods and zonal wave numbers of SW^+ and SW^- in the space-time domain that correspond to the pseudolongitude spectral peaks in Table 1. Thus, the (periods, zonal wave numbers) of SW that collapse onto $k_s = 1.16$ are (20.7 h, 0) for DE1, (11.1 h, 1) for S0, and (13.0 h, 3) for SW4. Note also that all Q6DW interactions with migrating tides (e.g., DW1 and SW2) are indistinguishable from the $k_s = |m - \delta| = 0.84$ Q6DW peak itself. There are other peaks in Figure 6 that likely arise from other PW-tide interactions; for instance, the peaks near 1.5 and 3.5 during February 2013, would be consistent with Q2DW-tide interactions [*Forbes and Moudden*, 2012].

It is informative to consider how the waves in Table 1 would be viewed from the ground, e.g., by a single radar or lidar. First, all of the primary and SW periods (28.6 h, 24.0 h, 20.7 h, 13.0 h, 12.0 h, 11.1 h) would be detectable, but observations from a single site would not be able to ascribe a zonal wave number or combination of zonal wave numbers to any one oscillation. At a given latitude, such a zonal wave number decomposition could in principle be performed if a sufficient number of observing sites were spread out in longitude; however, in practice, this type of coverage is not realized except perhaps for the lowest-order zonal wave numbers at a few latitudes. The complementary nature of ground-based and space-based measurements to reveal wave-wave nonlinear interactions is thus brought to light; ground-based measurements can reveal the sidebands around the frequencies of PW-modulated tides in the time domain, while the space-based measurements provide information on the aggregate contributions of all SW to the latitude versus longitude structure of the MLT.

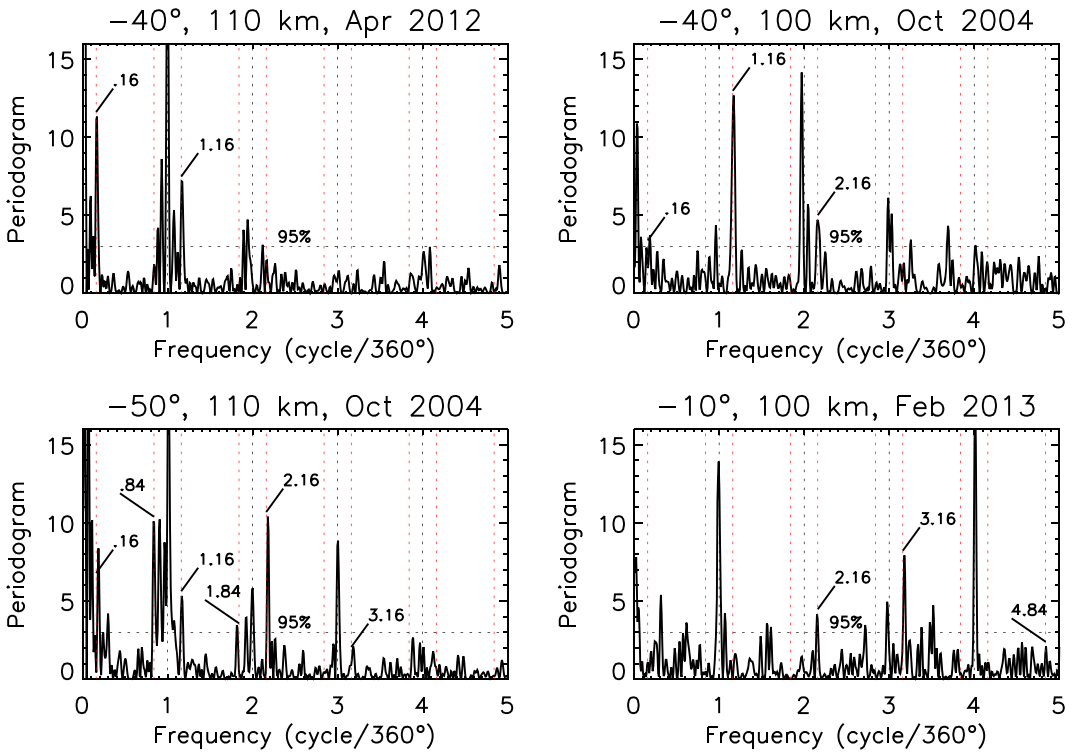

Figure 6. Typical examples of Lomb-Scargle pseudolongitude spectra for the SABER temperature residuals defined in section 2.1. Black vertical dashed lines at integer values correspond to nonmigrating tides with space-based zonal wave numbers as viewed from a quasi-Sun-synchronous satellite ($k_s = |n - s|$). The Q6DW and SW associated with Q6DW interactions with migrating tides all occur at $k_s = |m - \delta| = 0.84$ where $m = 1$ and $\delta = \frac{1}{6.14} = 0.16$ for the Q6DW. The red vertical dashed lines denote the k_s values consistent with Q6DW nonlinear interactions with nonmigrating tides and are given by $|(s - n) \pm (m - \delta)|$. Horizontal dashed lines correspond to the 95% confidence level.

Table 1. Locations of SW^+ and SW^- Pseudolongitude Spectral Peaks $k_s = |(s - n) \pm (m - \delta)|$ Corresponding to the Nonlinear Interactions of Various Solar Tidal Components With the Q6DW, Where Values of s and n are Given in the Table, and $m = 1$ and $\delta = 0.16$ for the Q6DW[a]

Tide	(s, n)	$\lvert s - n \rvert$	SW^+ (k_s, σ, s)	SW^- (k_s, σ, s)
DE3	−3,1	4	3.16, 20.7 h, −2	4.84, 28.6 h, −4
DE2	−2,1	3	2.16, 20.7 h, −1	3.84, 28.6 h, −3
DE1	−1,1	2	1.16, 20.7 h, 0	2.84, 28.6 h, −2
D0	0,1	1	0.16, 20.7 h, 1	1.84, 28.6 h, −1
DW1	1,1	0	0.84, 20.7 h, 2	0.84, 28.6 h, 0
DW2	2,1	1	1.84, 20.7 h, 3	0.16, 28.6 h, 1
SE2	−2,2	4	3.16, 11.1 h, −1	4.84, 13.0 h, −3
SE1	−1,2	3	2.16, 11.1 h, 0	3.84, 13.0 h, −2
S0	0,2	2	1.16, 11.1 h, 1	2.84, 13.0 h, −1
SW1	1,2	1	0.16, 11.1 h, 2	1.84, 13.0 h, 0
SW2	2,2	0	0.84, 11.1 h, 3	0.84, 13.0 h, 1
SW3	3,2	1	1.84, 11.1 h, 4	0.16, 13.0 h, 2
SW4	4,2	2	2.84, 11.1 h, 5	1.16, 13.0 h, 3

[a]Also included are the periods (σ) and zonal wave numbers (s) of the SW in the space-time domain.

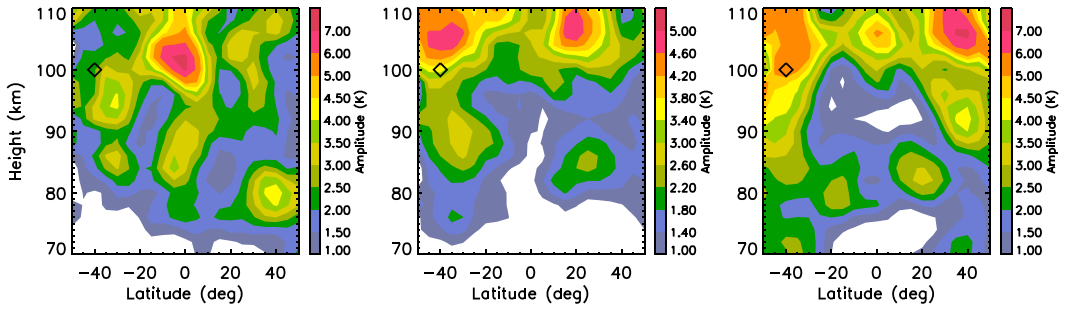

Figure 7. Space-based depictions of height versus latitude structures of some waves involved in nonlinear interactions, averaged over October 2004. (left) Combined contributions of DE1, S0, and SW4, seen as $k_s = |n - s| = 2$ in pseudolongitude spectra. (middle) Q6DW, seen as $k_s = 0.84$ in pseudolongitude spectra. (right) One of the SWs resulting from nonlinear interaction between the waves in Figures 7 (left) and 7 (middle), seen as $k_s = 1.16$ in pseudolongitude spectra.

The attributes of the space-based perspective are now more specifically revealed through example. Consider the above $k_s = 1.16$ peak associated with interaction of the Q6DW with DE1, S0, SW4. The space-based view of these waves, averaged for October 2004, are presented in Figure 7. Figure 7 (left) illustrates the combined contributions of DE1, S0, and SW4, which cannot be separated as noted above. Figure 7 (middle) depicts the combined contributions of the Q6DW plus any SW arising from Q6DW interactions with migrating tides. Figure 7 (right) represents the combined contributions of one set of SW (see Table 1) associated with nonlinear interaction between the Q6DW and the waves represented in Figure 7 (left). One important conclusion to draw from this figure is that the aggregate SW amplitudes are of the same order as the interacting primary waves (2–6 K). Moreover, since the SW have different latitude-height structures, periods, and zonal wave numbers than the interacting primary waves, they add to the overall *complexity* of the wave spectrum and any effects that it might have on the IT system.

Finally, it is possible to establish the temporal variability of the SW associated with the above interactions. Figure 8 depicts the latitude versus DOY variation of the $k_s = 1.16$ SW at 90 km throughout 2004. The SW maximizes (3–5 K) mainly at nonequatorial latitudes during March–May and August–November, similar to the broad climatological behavior of the Q6DW. As illustrated in Figure 8, consistent results are obtained using data from the ascending and descending parts of the TIMED orbit, validating the robustness of the results. It should be added that Figure 8 contains some irregular features of significant amplitude that are characteristic of other SW examined in the database. This is to be expected, since the SW derived from the above methodology are potentially composed of a superposition of SW from several PW-tide interactions, each one with its own latitude versus month distribution. The same applies to height versus latitude structures similar to those displayed in Figure 7.

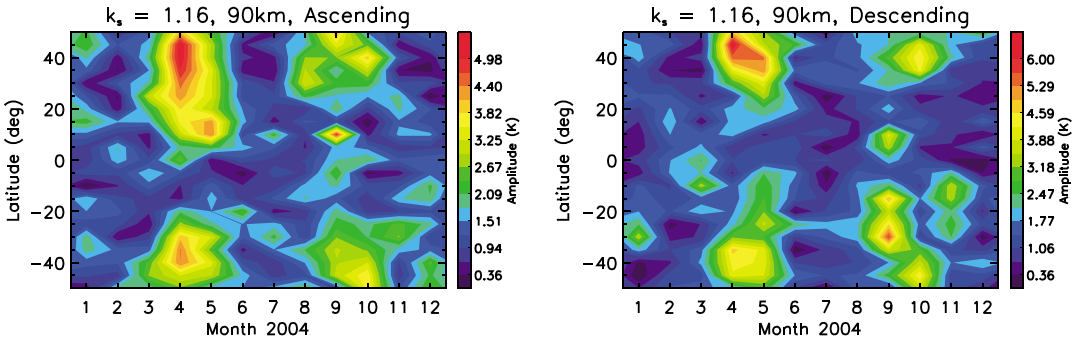

Figure 8. Latitude versus month depictions of $k_s = 1.16$ SW amplitudes at 90 km during 2004, ascending data on the left and descending data on the right.

5. Summary and Conclusions

One objective of the current work was to provide some new insights into the Q6DW through analysis of TIMED/SABER measurements between 20 and 110 km and ±50° latitude during 2012–2015. First, it is found that the Q6DW possesses a mean period of 6.14 days with a standard deviation of 0.26 day. In addition, the Q6DW in the MLT experiences significant interannual variability, ranging from weak (<3 K) global amplitudes during 2008 to rather strong amplitudes (8 K) in both hemispheres during 2004. Consistent with previous works [*Wu et al.*, 1994; *Talaat et al.*, 2001, 2002; *Lieberman et al.*, 2003; *Riggin et al.*, 2006; *Jiang et al.*, 2008; *Pancheva et al.*, 2009; *Gu et al.*, 2014], the latitudinal shape of the Q6DW is found to be broadly consistent with that of the 5 day normal mode, with relatively small amplitudes near the equator, maxima poleward of about ±30° latitude, and near-symmetry in amplitude and phase with respect to the equator.

The mean vertical amplitude structure of the Q6DW is close to that of a classical normal mode up to about 70 km, but significant deviations exist above this altitude. Downward phase progression with height with a vertical wavelength of about 70 km occurs between 40 and 100 km; this departure from the infinite vertical wavelength expected for a normal mode is an indication of dissipation of the wave. Finally, the occurrence of stratospheric Q6DW maxima during the course of the year are not well correlated with those in the MLT. All of these characteristics are consistent with the possible presence of an instability-driven or instability-amplified Q6DW in the MLT region as discussed in, e.g., *Meyer and Forbes* [1997] and *Lieberman et al.* [2003]. According to model simulations [*Liu et al.*, 2004], the seasonal-latitudinal MLT structure of the Q6DW originating at lower altitudes is determined by a complex interplay between the intervening zonal wind field and the conditions for instability that produce amplification of the wave. This interplay likely accounts for many of the seasonal-latitudinal and vertical structural features of the Q6DW revealed in this study.

The main objective of the present work is to provide the first comprehensive experimental evidence for Q6DW-tide interactions. This is prompted in part by recent numerical modeling by *Pedatella et al*. [2012] and *Gan et al.* [2016] which indicate the potential significance of Q6DW-tide interactions, the former focusing on interactions with DE2 and DE3 and the latter on DW1 and SW2. However, the methodology used to reveal the present of PW-tide interactions based on observations from a quasi-Sun-synchronous platform like TIMED [*Moudden and Forbes*, 2010] possesses some peculiarities that warrant some attention to place the current work in an informative context. The following summary of this aspect of our work aims to provide this context.

Evidence for nonlinear interactions between the Q6DW and various solar tides comes in the form of spectra (see Figure 6 for a few examples and Figures S2a–S2d for many more) of month-long sequences of ascending and descending temperature measurements at specific heights and latitudes as observed by the SABER instrument on the TIMED satellite from 2002 to 2015. The spectra are performed with respect to the sequence of points at "pseduolongitudes" sampled by SABER as the Earth rotates beneath the TIMED orbit, incremented by 2π each day from beginning to end of each month. Notable peaks occur in the pseudolongitude spectra at integer space-based zonal wave numbers $k_s = |n - s|$ that correspond to the presence of nonmigrating solar tides and at other distinct values $k_s = |n - s \pm 0.84|$ that correspond to SW that arise due to nonlinear interactions between the Q6DW and various solar tides (refer to Table 1). Other peaks in Figure S2 appear at $k_s = |n - s \pm 0.5|$ and $k_s = |n - s \pm 0.1|$, which arise as SW due to nonlinear interactions between the Q2DW and Q10DW, respectively.

Many of the peaks listed in Table 1 appear somewhere in the spectra of Figures S2a–S2d. It is important to note that all migrating tides ($s - n = 0$) collapse onto $k_s = 0$ and that all SW due to interactions between the Q6DW and all migrating tides collapse onto the spectral peak for the Q6DW itself, i.e., $k_s = 0.84$. Therefore, we are not able to comment on the potential significance of Q6DW interactions with migrating tides. Possible signatures of DE2 ($k_s = 2.16$) and DE3 ($k_s = 3.16$) appear in Figure 6, consistent with the findings of *Pedatella et al.* [2012], although these peaks could in principle be associated with SE1 ($k_s = 2.16$) and SE2 ($k_s = 3.16$) as well. There are also many spectra in Figures S2a–S2d that do not contain much evidence at all of significant PW-tide interactions, so it cannot be said that this process is ubiquitous in the MLT region.

The specific Q6DW-tide interactions that contribute to any given SW peak in the pseudolongitude spectra cannot be individually quantified since several values of s and n can combine to yield specific integral values of $(n - s)$. However, it is possible to determine the aggregate contributions of all interactions to a given SW peak by simply least squares fitting to determine the amplitude of k_s as a function of latitude and height over any given period of time. In the present work it is found that it is common for SW amplitudes to achieve

amplitudes of order 2–6 K, i.e., of similar amplitude to the Q6DW and nonmigrating tides in the 80–110 km height region. Specific examples for 2004 when the Q6DW was particularly well established are provided in Figures 7 and 8. The significance of this result is that the SW possess wave periods and zonal wave numbers different from the interacting (primary) waves, thus adding to both the spatial and temporal complexity of the wave spectrum. Since this wave spectrum is known to generate electric fields through the *E* region dynamo mechanism, then this complexity should extend to ground magnetic variations produced by Sq currents, and to the *F* region plasma redistributions produced by the electric fields [e.g., *Forbes*, 1996]. Similar complexity should also extend to the spatial-temporal variability that arises in connection with *E* region irregularities produced in connection with the tidal wind shear mechanism [*Mathews*, 1998; *Arras et al.*, 2008] and thus to the accompanying scintillations produced in GPS signals [*Chu et al.*, 2014].

The present work provides new experimental insights into the presence of PW-tide interactions. Aggregate amplitudes of the corresponding SW from the space-based perspective are quantified, leading to the conclusion that SW make a measurable contribution to the complexity of the wave spectrum entering the IT system. Such complexity is expected to permeate to the ionospheric plasma via direct transport and through the effects of dynamo electric fields. The present work would be complemented by analyses of ground-based data (e.g., of the type conducted by *Beard et al.* [1999] and *Pancheva* [2001]) that could identify the presence of SW in the time domain (i.e., wave periods of 11.1 h, 13.0 h, 20.7 h, and 28.6 h as given in Table 1). However, these would not be distinguishable from those produced by Q6DW interactions with migrating tides unless data from a longitude chain of observing stations is employed.

Acknowledgments
The authors gratefully acknowledge support for this work from NASA award NNX12AJ58G through the Heliophysics Guest Investigator Program and NSF grant AGS-1630177 under the ATM-Aeronomy Program. The TIMED/SABER data used in this study can be freely accessed at http://saber.gats-inc.com/data.php.

References

Arras, C., J. Wickert, G. Beyerle, S. Heise, T. Schmidt, and C. Jacobi (2008), A global climatology of ionospheric irregularities derived from GPS radio occultation, *Geophys. Res. Lett.*, *35*, L14809, doi:10.1029/2008GL034158.

Beard, A. G., N. J. Mitchell, P. J. S. Williams, and M. Kunitake (1999), Non-linear interactions between tides and planetary waves resulting in periodic tidal variability, *J. Atmos. Sol. Terr. Phys.*, *61*, 363–376.

Canziani, P. O. (1994a), On tidal variability and the existence of planetary wave-like oscillations in the upper thermosphere I. Observations of tidal variability, *J. Atmos. Sol. Terr. Phys.*, *56*, 901–902.

Canziani, P. O. (1994b), On tidal variability and the existence of planetary wave-like oscillations in the upper thermosphere II. Nonlinear interactions and global scale oscillations, *J. Atmos. Sol. Terr. Phys.*, *56*, 913–930.

Cevolani, G., and S. Kingsley (1992), Non-linear effects on tidal and planetary waves in the lower thermosphere: Preliminary results, *Adv. Space Res.*, *12*(10), 77–80.

Chu, Y. H., C. Y. Wang, K. H. Wu, K. T. Chen, K. J. Tzeng, C. L. Su, W. Feng, and J. M. C. Plane (2014), Morphology of sporadic *E* layer retrieved from COSMIC GPS radio occultation measurements: Wind shear theory examination, *J. Geophys. Res. Space Physics*, *119*, 2117–2136, doi:10.1002/2013JA019437.

Clark, R. R., and J. S. Bergin (1997), Bispectral analysis of mesosphere winds, *J. Atmos. Sol. Terr. Phys.*, *59*, 629–639.

Elhawary, R., and J. M. Forbes (2016), Planetary wave variability of Sq currents, *J. Geophys. Res. Space Physics*, *121*, 11,316–11,332, doi:10.1002/2016JA023242.

Espy, P. J., and G. Witt (1996), Observation of a quasi 16-day oscillation in the polar summer mesospheric temperature, *Geophys. Res. Lett.*, *23*, 1071–1074.

Forbes, J. M. (1995), Tidal and planetary waves (a tutorial), in *The Upper Mesosphere and Lower Thermosphere: A Review of Experiment and Theory, Geophys. Monogr. Ser.*, vol. 87, edited by R. M. Johnson and T. L. Killeen, pp. 67–87, AGU, Washington, D. C.

Forbes, J. M. (1996), Planetary waves in the thermosphere-ionosphere system, *J. Geomagn. Geoelectr.*, *48*, 91–98.

Forbes, J. M., and Y. Moudden (2012), Quasi-two-day wave-tide interactions as revealed in satellite observations, *J. Geophys. Res.*, *117*, D12110, doi:10.1029/2011JD017114.

Forbes, J. M., and X. Zhang (2015), Quasi-10-day wave in the atmosphere, *J. Geophys. Res. Atmos.*, *120*, 11,079–11,089, doi:10.1002/2015JD023327.

Forbes, J. M., X. Zhang, S. Palo, J. Russell, C. J. Mertens, and M. Mlynczak (2008), Tidal variability in the ionospheric dynamo region, *J. Geophys. Res.*, *113*, A02310, doi:10.1029/2007JA0127370.

Forbes, J. M., X. Zhang, S. Palo, J. Russell, M. Mlynczak, and C. J. Mertens (2009), Kelvin waves in stratosphere, mesosphere and lower thermosphere temperatures as observed by TIMED/SABER during 2002–2006, *Earth Planets Space*, *61*, 447–453.

Gan, Q., J. Yue, L. C. Chang, W. B. Wang, S. D. Zhang, and J. Du (2015), Observations of thermosphere and ionosphere changes due to the dissipative 6.5-day wave in the lower thermosphere, *Ann. Geophys.*, *33*(7), 913–922, doi:10.5194/angeo-33-913-2015.

Gan, Q., W. Wang, J. Yue, H. Liu, L. C. Chang, S. Zhang, A. Burns, and J. Du (2016), Numerical simulation of the 6 day wave effects on the ionosphere: Dynamo modulation, *J. Geophys. Res. Space Physics*, *121*, 10,103–10,116, doi:10.1002/2016JA022907.

Gu, S. Y., H. L. Liu, T. Li, X. K. Dou, Q. Wu, and J. M. Russell (2014), Observation of the neutral-ion coupling through 6 day planetary wave, *J. Geophys. Res. Space Physics*, *119*, 10,376–10,383, doi:10.1002/2014JA020530.

Gasperini, F., J. M. Forbes, E. N. Doornbos, and S. L. Bruinsma (2015), Wave coupling between the lower and middle thermosphere as viewed from TIMED and GOCE, *J. Geophys. Res. Space Physics*, *120*, 5788–5804, doi:10.1002/2015JA021300.

Hirooka, T., and I. Hirota (1984), Normal mode Rossby waves observed in the upper stratosphere, Part 2: Second symmetric modes of zonal wavenumbers 1 and 2, *J. Atmos. Sci.*, *41*, 536–548.

Huuskonen, A., T. S. Virdi, G. O. L. Jones, and P. J. S. Williams (1991), Observations of day-to-day variability in the meridional semi-diurnal tide at 70°N, *Ann. Geophys.*, *9*, 407–415.

Jiang, G., et al. (2008), A case study of the mesospheric 6.5-day wave observed by radar systems, *J. Geophys. Res.*, *113*, D16111, doi:10.1029/ 2008JD009907.

Lieberman, R. S., D. M. Riggin, S. J. Franke, A. H. Manson, C. Meek, T. Nakamura, T. Tsuda, R. A. Vincent, and I. Reid (2003), The 6.5-day wave in the mesosphere and lower thermosphere: Evidence for baroclinic/barotropic instability, *J. Geophys. Res.*, *108*(D20), 4640, doi:10.1029/2002JD003349.

Lindzen, R. S., and D. Blake (1972), Lamb waves in the presence of realistic distributions of temperature and dissipation, *J. Geophys. Res.*, *77*, 2166–2176.

Liu, H.-L., E. R. Talaat, R. G. Roble, R. S. Lieberman, D. M. Riggin, and J.-H. Yee (2004), The 6.5-day wave and its seasonal variability in the middle and upper atmosphere, *J. Geophys. Res.*, *109*, D21112, doi:10.1029/2004JD004795.

Liu, G., T. J. Immel, S. L. England, K. K. Kumar, and G. Ramkumar (2010), Temporal modulations of the longitudinal structure in F2 peak height in the equatorial ionosphere as observed by COSMIC, *J. Geophys. Res.*, *115*, A04303, doi:10.1029/2009JA014829.

Longuet-Higgins, M. S. (1968), The eigenfunctions of Laplace's tidal equations over a sphere, *Philos. Trans. R. Soc. A*, *262*, 511–607, doi:10.1098/rsta.1968.0003.

Mathews, J. D. (1998), Sporadic E: Current views and recent progress, *J. Atmos. Sol. Terr. Phys.*, *60*(4), 413–435.

Mertens, C. J., M. G. Mlynczak, M. López-Puertas, P. P. Wintersteiner, R. H. Picard, J. R. Winick, and L. L. Gordley (2001), Retrieval of mesospheric and lower thermospheric kinetic temperature from measurements of CO_2 15 μm Earth limb emission under non-LTE conditions, *Geophys. Res. Lett.*, *28*(7), 1391–1394.

Meyer, C. K., and J. M. Forbes (1997), A 6.5-day westward propagating planetary wave: Origin and characteristics, *J. Geophys. Res.*, *102*, 26,173–26,178.

Miyoshi, Y. (1999), Numerical simulation of the 5-day and 16-day waves in the mesopause region, *Earth Planets Space*, *51*, 763–772.

Moudden, Y., and J. M. Forbes (2010), A new interpretation of Mars aerobraking variability: Planetary wave-tide interactions, *J. Geophys. Res.*, *115*, E09005, doi:10.1029/2009JE003542.

Moudden, Y., and J. M. Forbes (2011a), Simulated planetary wave-tide interactions in the atmosphere of Mars, *J. Geophys. Res.*, *116*, E01004, doi:10.1029/2010JE003698.

Moudden, Y., and J. M. Forbes (2011b), First detection of wave interactions in the middle atmosphere of Mars, *Geophys. Res. Lett.*, *38*, L04202, doi:10.1029/2010GL045592.

Moudden, Y., and J. M. Forbes (2014), Quasi-two-day wave structure, interannual variability, and tidal interactions during the 2002–2011 decade, *J. Geophys. Res. Atmos.*, *119*, 2241–2260, doi:10.1002/2013JD020563.

Pancheva, D. (2001), Non-linear interaction of tides and planetary waves in the mesosphere and lower thermosphere: Observations over Europe, *Phys. Chem. Earth, Part C*, *26*, 411–418.

Pancheva, D. (2006), Quasi-2-day wave and tidal variability observed over Ascension Island during January/February 2003, *J. Atmos. Sol. Terr. Phys.*, *68*, 390–407.

Pancheva, D., P. Mukhatrov, N. Mitchell, D. Fritts, D. Riggin, H. Takahashi, P. Batista, B. Clemesha, S. Gurubaran, and G. Ramkumar (2008), Planetary wave coupling (5–6-day waves) in the low latitude atmosphere-ionosphere system, *J. Atmos. Sol. Terr. Phys.*, *70*, 101–122.

Pancheva, D., P. Mukhtarov, B. Andonov, N. J. Mitchell, and J. M. Forbes (2009), Planetary waves observed by TIMED/SABER in coupling the stratosphere-mesosphere-lower thermosphere during the winter of 2003/2004: Part 2, Altitude and latitude planetary wave structure, *J. Atmos. Sol. Terr. Phys.*, *71*, 75–87.

Pedatella, N. M., and J. M. Forbes (2012), The quasi-two day wave and spatial-temporal variability of the OH emission and ionosphere, *J. Geophys. Res.*, *117*, A01320, doi:10.1029/2011JA017186.

Pedatella, N. M., H.-L. Liu, and M. E. Hagan (2012), Day-to-day migrating and nonmigrating tidal variability due to the six-day planetary wave, *J. Geophys. Res.*, *117*, A06301, doi:10.1029/2012JA017581.

Pancheva, D. V., and N. J. Mitchell (2004), Planetary waves and variability of the semidiurnal tide in the mesosphere and lower thermosphere over Esrange (68°N, 21°E) during winter, *J. Geophys. Res.*, *109*, A08307, doi:10.1029/2004JA010433.

Remsberg, E. E., et al. (2008), Assessment of the quality of the version 1.07 temperature-versus-pressure profiles of the middle atmosphere TIMED/SABER, *J. Geophys. Res.*, *113*, D17101, doi:10.1029/2008JD010013.

Riggin, D. M., et al. (2006), Observations of the 5-day wave in the mesosphere and lower thermosphere, *J. Atmos. Sol. Terr. Phys.*, *68*, 323–329.

Salby, M. (1981), Rossby normal modes in nonuniform background configurations. Part II: Equinox and solstice conditions, *J. Atmos. Sci.*, *38*, 1827–1840.

Salby, M. L. (1979), On the solution of the homogeneous vertical structure problem for long-period oscillations, *J. Atmos. Sci.*, *36*, 2350–2359.

Sassi, F., R. R. Garcia, and K. W. Hoppel (2012), Large-scale Rossby normal modes during some recent Northern Hemisphere winters, *J. Atmos. Sci.*, *69*, 820–839.

Sassi, F., H.-L. Liu, J. Ma, and R. R. Garcia (2013), The lower thermosphere during the Northern Hemisphere winter of 2009: A modeling study using high-altitude data assimilation products in WACCM-X, *J. Geophys. Res. Atmos.*, *118*, 8954–8968, doi:10.1002/jgrd.50632.

Talaat, E. R., J. H. Yee, and X. Zhu (2001), Observations of the 6.5-day wave in the mesosphere and lower thermosphere, *J. Geophys. Res.*, *106*, 20,715–20,723.

Talaat, E. R., J.-H. Yee, and X. Zhu (2002), The 6.5-day wave in the tropical stratosphere and mesosphere, *J. Geophys. Res.*, *107*(D12), 4133, doi:10.1029/2001JD000822.

Teitelbaum, H., and F. Vial (1991), On tidal variability induced by nonlinear interaction with planetary waves, *J. Geophys. Res.*, *96*, 14,169–14,178.

Truskowski, A. O., J. M. Forbes, X. Zhang, and S. E. Palo (2014), New perspectives on thermosphere tides—1. Lower thermosphere spectra and seasonal-latitudinal structures, *Earth Planets Space*, *66*, 136, doi:10.1186/s40623-014-0136-4.

Tunbridge, V. M., D. J. Sandford, and N. J. Mitchell (2011), Zonal wave numbers of the summertime 2 day planetary wave observed in the mesosphere by EOS Aura Microwave Limb Sounder, *J. Geophys. Res.*, *116*, D11103, doi:10.1029/2010JD014567.

Wu, D. L., P. B. Hays, and W. R. Skinner (1994), Observations of the 5-day wave in the mesosphere and lower thermosphere, *Geophys. Res. Lett.*, *21*, 2733–2736.